J Mater Sci: Mater Electron (2026) 37:400

Structural, electrical transport and magnetic properties of palladium (II) chloride added $Bi_{1.6}Pb_{0.4}Sr_2CaCu_2O_8$ superconductor

M. A. Salma[1], A. B. P. Ilhamsyah[2], R. Abd-Shukor[2], N. Mohd Hapipi[1], M. M. Awang Kechik[1], K. P. Lim[1], R. Che Hak[3], H. Baqiah[4], and S. K. Chen[1,5,*]

[1] *Superconductor and Thin Film Laboratory, Department of Physics, Faculty of Science, Universiti Putra Malaysia, 43400 Serdang, Selangor, Malaysia*

[2] *Department of Applied Physics, Universiti Kebangsaan Malaysia, 43600 Bangi, Selangor, Malaysia*

[3] *Malaysian Nuclear Agency, Kajang, 43000 Bangi, Selangor, Malaysia*

[4] *Shandong Key Laboratory of Biophysics, Institute of Biophysics, Dezhou University, University Rd. West, No.566, Dezhou, Shandong, China*

[5] *Institute of Nanoscience and Nanotechnology (ION2), Universiti Putra Malaysia, 43400 Serdang, Selangor, Malaysia*

Received: 31 October 2025
Accepted: 8 February 2026

ABSTRACT

In this study, the effect of palladium (II) chloride ($PdCl_2$) addition on the structural, microstructural, and superconducting properties of $Bi_{1.6}Pb_{0.4}Sr_2CaCu_2O_8$ (Bi-2212) was investigated. X-ray diffraction (XRD) confirmed Bi-2212 as the dominant phase in all samples. The incorporation of $PdCl_2$ led to a reduction in both lattice parameters and unit cell volume. Scanning electron microscopy (SEM) revealed platy grains in $PdCl_2$-added samples compared to the pure one. Both the onset transition temperature ($T_{c\,onset}$) and magnetic susceptibility transition temperature ($T_{c\chi'}$) improved with $PdCl_2$ addition. The 0.4 wt% $PdCl_2$-added sample exhibited the highest $T_{c\,onset}$ of 96 K and a zero-resistance transition temperature ($T_{c\,zero}$) of 77 K. AC susceptibility measurements showed that samples with $x = 1.0$ and 1.5 wt% $PdCl_2$ exhibited the highest $T_{c\chi'}$ of 86 K. The 0.4 wt% $PdCl_2$-added sample also showed the highest intergrain loss peak temperature (T_{p2}), indicating enhanced flux pinning strength. $PdCl_2$ addition influenced crystallite size, which contributed to the improved superconducting performance of Bi-2212 phase. These results demonstrated that the decreased crystallite size due to the $PdCl_2$ addition may have induced defects that serve as effective flux pinning center of Bi-2212 superconductor.

Address correspondence to E-mail: chensk@upm.edu.my

https://doi.org/10.1007/s10854-026-16795-y
Published online: 20 February 2026

1 Introduction

The bismuth-strontium-calcium-copper-oxide (BSCCO) family is one of the well-known high-temperature superconductors (HTS). These cuprate superconductors are characterized by their layered perovskite-like structures, comprising alternating CuO_2 planes and charge reservoir layers, which play a crucial role in their superconducting behavior [1]. The general chemical formula for the Bi-based superconductors can be represented as $Bi_2Sr_2Ca_{n-1}Cu_nO_{2n+4+\delta}$ (where $n = 1$, 2, or 3), corresponding to the $Bi_2Sr_2CuO_{6+\delta}$ (Bi-2201), $Bi_2Sr_2CaCu_2O_{8+\delta}$ (Bi-2212), and $Bi_2Sr_2Ca_2Cu_3O_{10+\delta}$ (Bi-2223) phases, respectively. Each phase differs by the number of CuO_2 planes per unit cell, with higher n values typically leading to higher superconducting transition temperature (T_c) [2]. It is widely known that appropriate Pb substitution in Bi-based superconductors results in the formation of single-phase samples with significantly enhanced T_c [3, 4].

One of the interesting family of Bi-based superconductors is the $Bi_{1.6}Pb_{0.4}Sr_2CaCu_2O_8$. It consists of double CuO_2 layers and exhibits superconductivity in the range of 80—85 K. Compared to the Bi-2223, the Bi-2212 phase can be more easily formed with appropriate heat treatment [5, 6]. Under identical thermal conditions during the synthesis process, the oxygen stoichiometry of Bi-2212 remains relatively invariant with respect to cationic additions [7]. In addition, Bi-2212 can achieve a critical current density (J_c), in the order of 10^5 A·cm^{-2} at low temperatures, remains stable over a wide temperature range, and exhibits reduced weak-link problems compared to Bi-2223 [8, 9]. It also shows relatively higher J_c and irreversibility field under an applied magnetic field compared to the Bi-2223 phase [9, 10]. These favorable properties make Bi-2212 suitable for applications such as power cables and magnetic resonance imaging (MRI) systems [8, 11, 12].

However, cuprate-based superconductors suffer from weak intergranular coupling, pronounced anisotropy, and short coherence lengths, which limit their technological potential [13]. This is no exception for Bi-based superconductor systems, where poor mechanical properties further exacerbate these challenges [14, 15]. Substitution or addition of elements and compounds has been one of the simplest and most promising approaches to address these limitations.

The additions of palladium (Pd) and chlorine (Cl) (elements or compounds) to cuprate superconductors have been studied, revealing interesting results. In $SmBa_2Cu_3O_7$ superconductors, the addition of small amount of Pd resulted in improvement of T_c (~ 89 K) and J_c (10^4 A·cm^{-2}) [16]. In contrast, Pd-doped $Bi_{1.7}Pb_{0.3}Sr_2Ca_2Cu_3O_{10}$ (Bi-2223) exhibited suppression of Bi-2223 phase formation, a lower T_c, and no enhancement in flux pinning capability [17]. Similarly, Pd addition in $YBa_2Cu_3O_7$ superconductors produced no substantial changes in superconducting properties [18].

For Cl-containing compounds, the addition of $KClO_3$ to YBCO superconductor resulted in the highest T_c compared to K_2CO_3 and the undoped sample [19]. Substitution of KCl at Ba site in YBCO led to increase grain size, T_c, and magnetic susceptibility [20]. In Cl-added YBCO thin films, the texture, density, and J_c were improved, despite no significant change in T_c [21]. The additions of $BiCl_3$, BiOCl, $CaCl_2$, $SrCl_2$ and $LiClO_4$ into Bi-2212 superconductor have been studied [22]. It was shown that the addition of $LiClO_4$ into Bi-2212 increased T_c and promoted Bi-2212 phase formation at lower synthesis temperature. AC susceptibility measurement of the Bi-2223 added with LiCl showed an anomalous suppression of T_c which is due to the charge ordering phenomenon [23].

To date, the effect of metal chloride on $Bi_{1.6}Pb_{0.4}Sr_2CaCu_2O_8$ (Bi-2212) superconductors has not been extensively studied. Considering the beneficial effect of Pd and Cl-containing compounds on cuprate superconductors, this work investigates the influence of palladium (II) chloride ($PdCl_2$) addition on the superconductivity of Bi-2212. $PdCl_2$ is a paramagnetic compound commonly used as a catalyst in organic synthesis [24, 25], with a melting point of 678–680 °C, which is lower than the formation temperature of Bi-2212 phase (800–820 °C). At elevated temperatures, $PdCl_2$ decomposes into Pd and Cl [26], allowing both elements to interact with the Bi-2212 matrix, and potentially improve the superconducting performance. Therefore, the motivation of this study is to investigate the effect of $PdCl_2$ addition on the structural, electrical and magnetic properties of $Bi_{1.6}Pb_{0.4}Sr_2CaCu_2O_8$ superconductor.

2 Experimental details

Samples with the nominal composition $Bi_{1.6}Pb_{0.4}Sr_2CaCu_2O_8$ were synthesised via the solid-state reaction method. High-purity (≥ 99.9%)

precursors of bismuth oxide (Bi_2O_3), lead oxide (PbO), calcium oxide (CaO), copper oxide (CuO) and strontium carbonate (Sr_2CO_3) were weighed according to the stoichiometric ratio of 1.6: 0.4: 2.0: 1.0: 2.0 for Bi: Pb: Sr: Ca: Cu. The powders were thoroughly mixed and ground using an agate mortar and pestle, followed by calcination at 800 °C for 24 h with two intermediate grinding steps. A second calcination was then carried out at 840 °C for 50 h. After calcination, different weight percentages of $PdCl_2$ ($x = 0.0$, 0.1, 0.2, 0.4, 0.5. 1.0, 1.5 and 3.0 wt%) were added to the calcined powders. The resulting mixtures were pressed into circular pellets of approximately 2 mm in thickness and a diameter of 12.5 mm using a hydraulic press, followed by sintering at 840 °C for 24 h in air.

The crystalline phases of the samples were characterised using x-ray diffraction (XRD) with a Philips PW 3040/60 MPD X'pert High Pro Panalytical diffractometer equipped with a CuK_a radiation source ($\lambda = 1.5406$ Å). The scans were performed over a 2θ range of 4°–60°. The lattice parameters of the Bi-2212 phase were refined via Pawley refinement using the software X'pert HighScore. The volume fraction of Bi-2212 and Bi-2201 phase was determined using the equations:

$$V_{\text{Bi - 2212}} = \frac{\sum I_{\text{Bi - 2212}}}{\sum I_{\text{Bi - 2212}} + \sum I_{\text{Bi - 2201}} + \sum I_{Ca_2PbO_4} + \sum I_{Cu_8Sr_6O_z}} \times 100 \quad (1)$$

$$V_{\text{Bi - 2201}} = \frac{\sum I_{\text{Bi - 2201}}}{\sum I_{\text{Bi - 2212}} + \sum I_{\text{Bi - 2201}} + \sum I_{Ca_2PbO_4} + \sum I_{Cu_8Sr_6O_z}} \times 100 \quad (2)$$

where $\sum I_{\text{Bi-2212}}$ and $\sum I_{\text{Bi-2201}}$ represent the summed XRD peak intensities of the respective phases.

The surface morphology and elemental composition of the samples were examined using a scanning electron microscope (SEM, JEOL JSM 6400) equipped with an Oxford Instruments X-Max energy-dispersive X-ray spectroscopy (EDX) detector. Temperature-dependent electrical resistance measurements were carried out using the standard four-point probe method. For low-temperature measurements, a Keithley 197 Autoranging Microvolt DMM and a Keithley 220 Current Source were used in conjunction with a CTI Cryogenics Model 22 cryostat and a Lake Shore Model 340 temperature controller. A constant current source in the range of 1 – 100 mA was applied during the measurements. The room temperature resistivity (ρ_{298} K) was determined using the Van der Pauw method. AC susceptibility, ACS ($\chi = \chi' + i\chi''$) measurements were performed on the bar-shaped samples using a Cryo Industries REF-1808-AS susceptometer. The applied magnetic field and frequency was 5 Oe and 295 Hz, respectively.

3 Results and discussion

3.1 XRD analysis

Figure 1a and b show the XRD patterns of $Bi_{1.6}Pb_{0.4}Sr_2CaCu_2O_8$ samples with x wt% $PdCl_2$ additions ($x = 0.0$–3.0 wt%). All samples exhibited Bi-2212 as the major phase, along with Ca_2PbO_4 and $Bi_2Sr_2CuO_5$ (Bi-2201) as secondary impurity phases. The (hkl) indices of the Bi-2201 peaks are denoted by parentheses in the XRD patterns. The main diffraction peak corresponding to the Ca_2PbO_4 phase was observed at $2\theta = 17°$ in all the samples. For $PdCl_2$ additions ≥ 1 wt%, a new diffraction peak appeared at $2\theta = 14.26°$, corresponding to $Cu_8Sr_6O_z$ phase, and its intensity increased with increasing $PdCl_2$ addition. Generally, the volume fraction of Bi-2212 phase reduced after $PdCl_2$ addition (Table 1). This phase reduction became more pronounced at higher $PdCl_2$ addition ($x = 1.0$–3.0 wt%). This suggests that excess addition of $PdCl_2$ hinders the formation of Bi-2212 phase while aided the formation of impurity phase.

The Bi-2212 phase was indexed based on its tetragonal structure (PDF-00–040-0378) and the lattice parameters were refined using Pawley fitting using the X'pert HighScore software. The experimental and refined XRD patterns for samples with x = 0.0, 0.5 and 3.0 wt% samples are shown in Fig. 1. The R-factor (R_{wp}, R_{exp}, and R_p) and goodness of fitting χ^2 criteria were used to ascertain the measurement's validity. The refined lattice parameters for pure samples (0.0 wt%) were a = b = 5. 3991 Å and c = 30.810 Å. In general, all $PdCl_2$-added samples exhibited slightly lower lattice parameters and unit cell

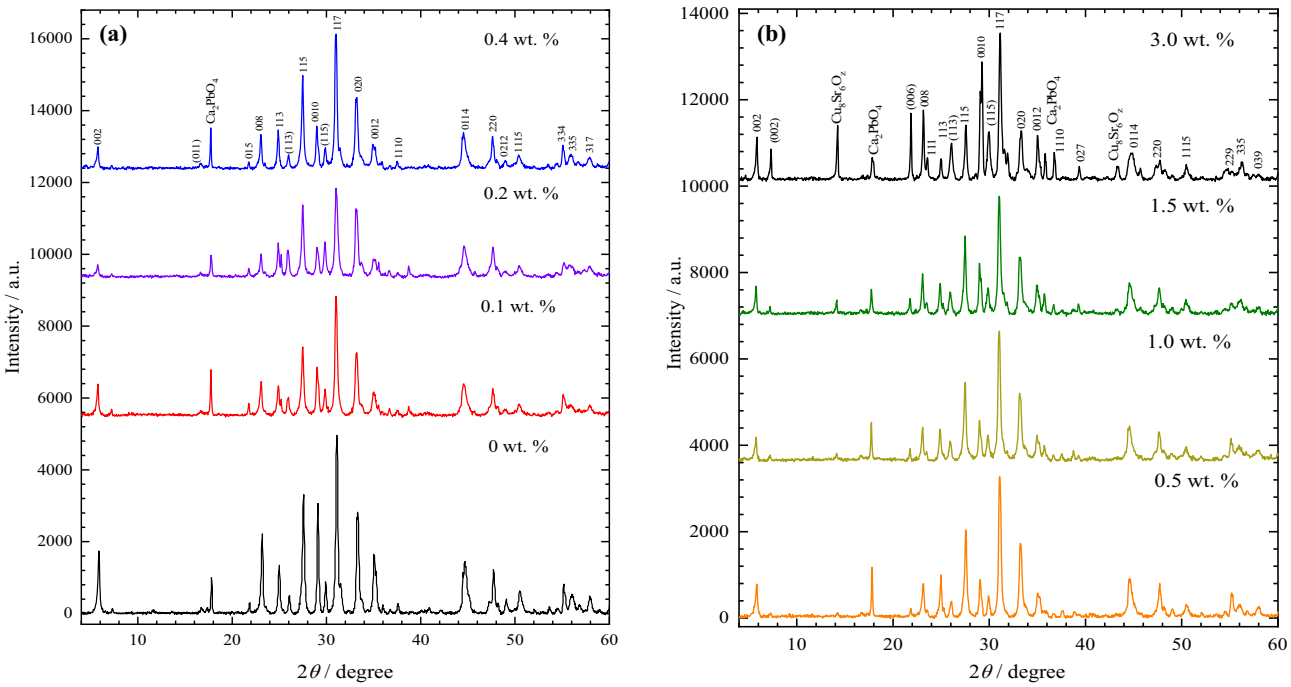

Fig. 1 **a** XRD patterns of $Bi_{1.6}Pb_{0.4}Sr_2CaCu_2O_8$ samples with *x* wt% $PdCl_2$ additions **b** XRD patterns of $Bi_{1.6}Pb_{0.4}Sr_2CaCu_2O_8$ samples with *x* wt% $PdCl_2$ additions

Table 1 Structural parameters of $Bi_{1.6}Pb_{0.4}Sr_2CaCu_2O_8$ samples with *x* wt% $PdCl_2$ additions

Sample/wt%	Lattice parameter		V/Å^3	Crystallite Size, D/ nm	Volume fraction/ %				Pawley fit parameter			
	a/Å	c/Å			Bi-2212	Bi-2201	Ca_2PbO_4	$Cu_8Sr_6O_z$	R_p/ %	R_{wp}/ %	R_{exp}/ %	χ^2
0	5.3991(3)	30.810(2)	898.12(16)	77.6	80	11	9	-	5.65	7.61	3.69	2.06
0.1	5.3937(5)	30.762(4)	894.93(28)	50.4	78	13	9	-	4.32	6.03	3.52	1.71
0.2	5.3924(1)	30.728(8)	893.51(27)	53.3	81	10	9	-	4.68	6.42	3.73	1.72
0.4	5.3933(5)	30.742(3)	894.21(25)	48.8	71	20	9	-	4.43	6.00	3.59	1.67
0.5	5.3939(5)	30.766(4)	895.11(28)	45.7	76	17	6	-	4.43	5.96	3.67	1.63
1.0	5.3935(8)	30.758(5)	894.75(41)	59.9	66	19	9	6	4.14	5.53	3.56	1.55
1.5	5.3922(6)	30.759(4)	894.34(32)	48.2	69	15	11	5	4.30	5.77	3.54	1.63
3.0	5.3907(4)	30.805(3)	895.18(22)	46.6	63	19	8	10	5.11	7.29	3.52	2.07

volumes compared to undoped sample. This demonstrated that the Pd ions might be substituted into the crystal structure of Bi-2212 phase. It was reported that Pd was substituted at Cu site of the Pd doped YBCO superconductor [27, 28]. In LiCl-added Bi-2223 superconductor, it was proposed that Li^+ ions, rather than Cl^-, entered the lattice due to the relatively large ionic radius of Cl^-, which makes its incorporation into the Bi-based lattice difficult [23]. In view of the decrease in both *a*- and *c*-axis after additions of $PdCl_2$ (Table 1), it is likely that the smaller Pd^{2+} (0.86 Å) substituted the bigger Ca^{2+} (1 Å). Moreover, this is favoured by the fact that the difference in ionic radius between Pd^{2+} and Ca^{2+} is smaller as compared to that between Pd^{2+} and Sr^{2+} (1.18 Å). The ionic radius of Cu^{2+} (0.73 Å) is smaller than that of Pd^{2+} [29].

The average crystallite size was determined using the Scherrer equation [30]:

$$D = \frac{K\lambda}{\beta_{hkl}\cos\theta} \tag{3}$$

where D represents the crystallite size, K is the shape factor (0.9), β_{hkl} is the full width at half maximum (FWHM) of the diffraction peak in radians, λ is the wavelength of CuK_α radiation (0.15406 nm), and θ is the Bragg angle corresponding to the selected (hkl) plane. The FWHM values of the (002), (008), (113), (115), and (117) reflections of the Bi-2212 phase were used for analysis. It was observed that $PdCl_2$ addition caused the decrease of the average crystallite size of Bi-2212 phase for all added samples (Table 1).

3.2 Microstructural analysis

Figure 2 shows the microstructures of $Bi_{1.6}Pb_{0.4}Sr_2CaCu_2O_8$ samples with x wt% $PdCl_2$ additions ($x = 0.0$, 0.2 and 0.4 wt%). All samples revealed randomly oriented plate-like grains, which are characteristics of the Bi-2212 phase owing to its layered crystal structure. With $PdCl_2$ addition, plate-like grains became more apparent indicating improved alignment compared to the undoped sample, suggesting that $PdCl_2$ facilitates enhanced intergranular connectivity and potentially promotes more effective supercurrent transport.

The EDX spectra of all samples are shown in Fig. 3, where peaks corresponding to Bi, Pb, Sr, Ca, Cu and O were detected in each sample. The Pd peak start to appear in the $x = 0.4$ wt% $PdCl_2$-added sample, likely due to the small amount of $PdCl_2$ addition resulting in the Pd signal falling below the detection threshold of EDX. The corresponding elemental compositions of each sample are shown in the insets of Figs. 3a–c. The measured atomic ratios of Bi: Pb: Sr: Ca: Cu: O slightly deviated from the ideal Bi-2212 stoichiometry, possibly due to the presence of secondary phases such as Bi-2201 and Ca_2PbO_4, as well as the limited sensitivity of EDX toward light elements like Cl and O.

Elemental mapping distributions of Bi, Sr, Ca, Cu, O, Pd and Cl on the surfaces of the $x = 0.2$ and 0.4 wt% samples are shown in Fig. 4, 5, respectively. Localised

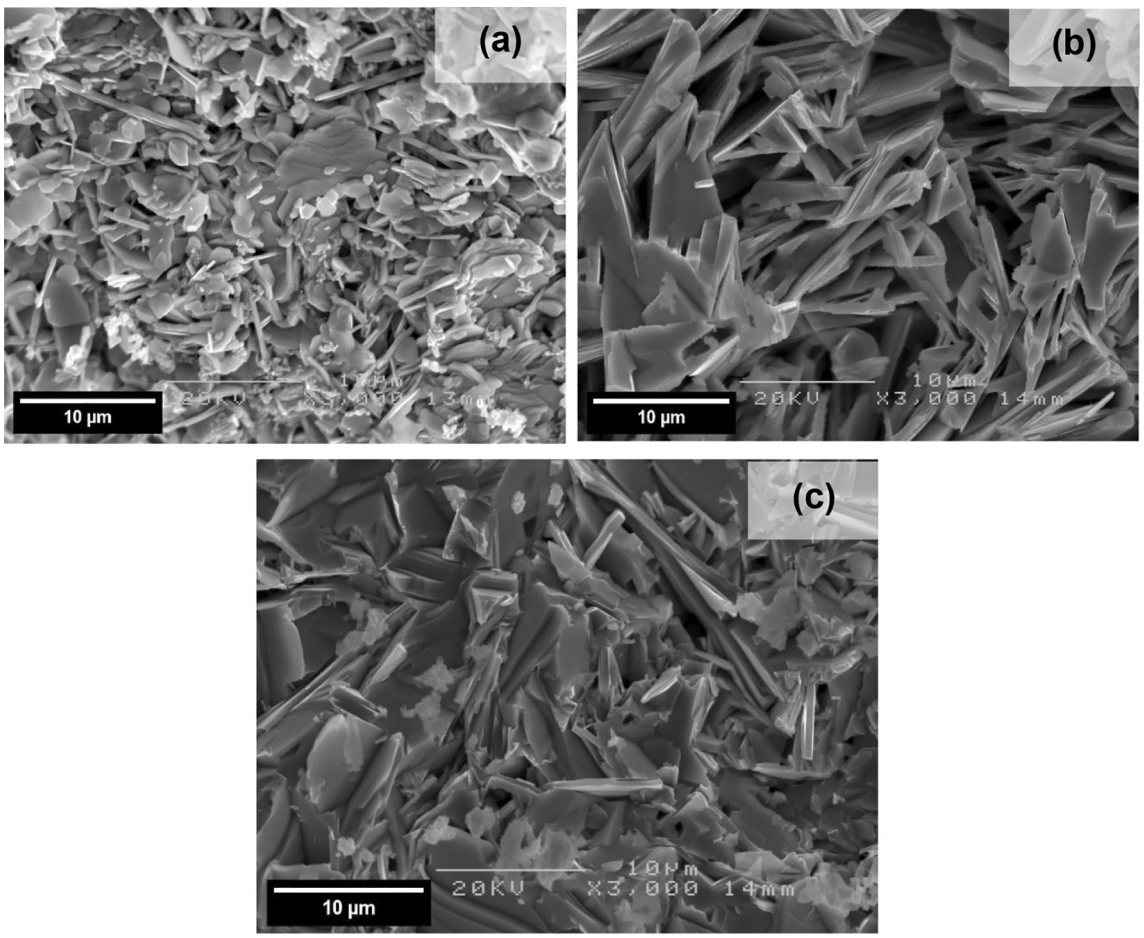

Fig. 2 SEM images of $Bi_{1.6}Pb_{0.4}Sr_2CaCu_2O_8$ samples added with **a** 0.0 wt%, **b** 0.2 wt% and **c** 0.4 wt% of $PdCl_2$ additions

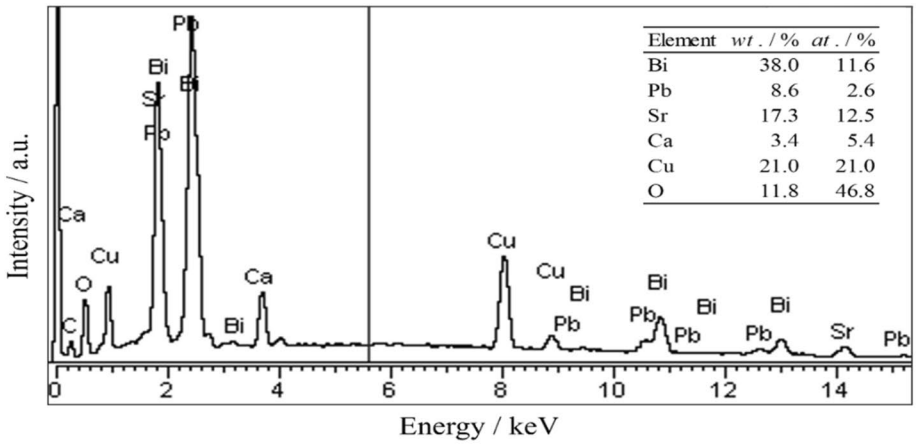

Fig. 3 EDX spectra of $Bi_{1.6}Pb_{0.4}Sr_2CaCu_2O_8$ samples added with **a** 0.0 wt%, **b** 0.2 wt% and **c** 0.4 wt% of $PdCl_2$ additions

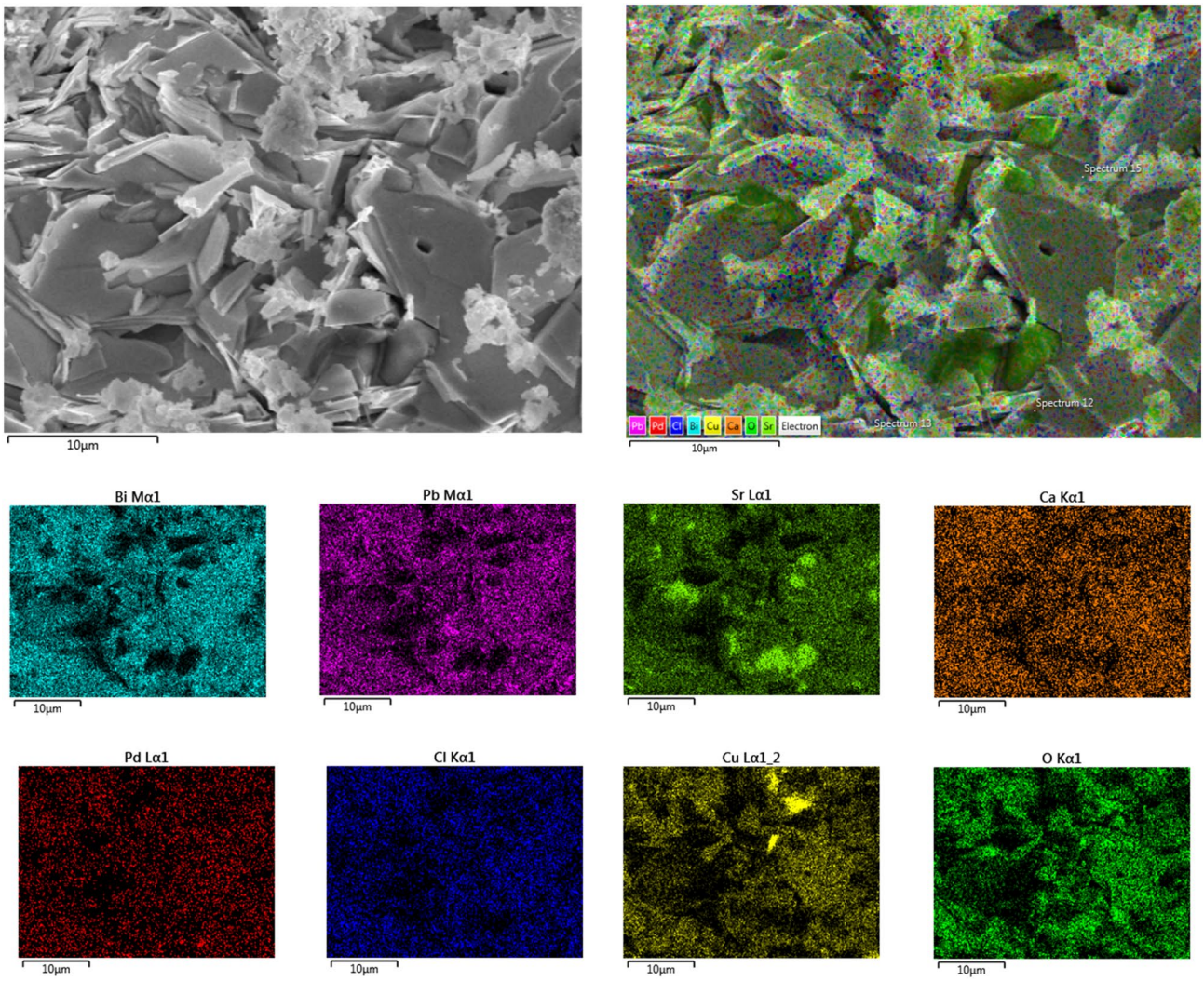

Fig. 4 Elemental distribution map of $Bi_{1.6}Pb_{0.4}Sr_2CaCu_2O_8$ added with 0.2 wt% $PdCl_2$

enrichment of Sr and Cu was observed in certain regions of the 0.2 wt% $PdCl_2$-added sample, while higher Pd and Cu concentrations were detected in specific areas of the 0.4 wt% $PdCl_2$-added sample. This may be attributed to an inhomogeneous distribution of $PdCl_2$ within Bi-2212 matrix, leading to localised accumulation of certain elements. Another possible explanation is the fluctuation in diffusion rates during heat treatment, phase separation at higher $PdCl_2$ contents, or incomplete mixing of precursor powders prior to sintering.

3.3 Temperature dependence of electrical resistance measurement

Figure 6 shows the temperature dependence of electrical resistance for all samples. The resistance was normalized to that at room temperature. The hump between 170 to 285 K in the plot for the 3.0 wt% $PdCl_2$ added sample was due to problem related to the measuring instrument or the electrical contact between the probe and the sample. One such possibility being that the silver paste used to make the electrical contact was not dried enough before the measurement was carried out. Most samples exhibited metallic behavior in the normal state above the onset transition temperature ($T_{c\ onset}$), except for 0.1 wt% and 0.2 wt% $PdCl_2$-added samples, which displayed semimetal-like behavior above $T_{c\ onset}$. This suggests that $PdCl_2$ addition at these concentrations may have modified the oxygen content or carrier concentration in the Bi-2212 phase [14].

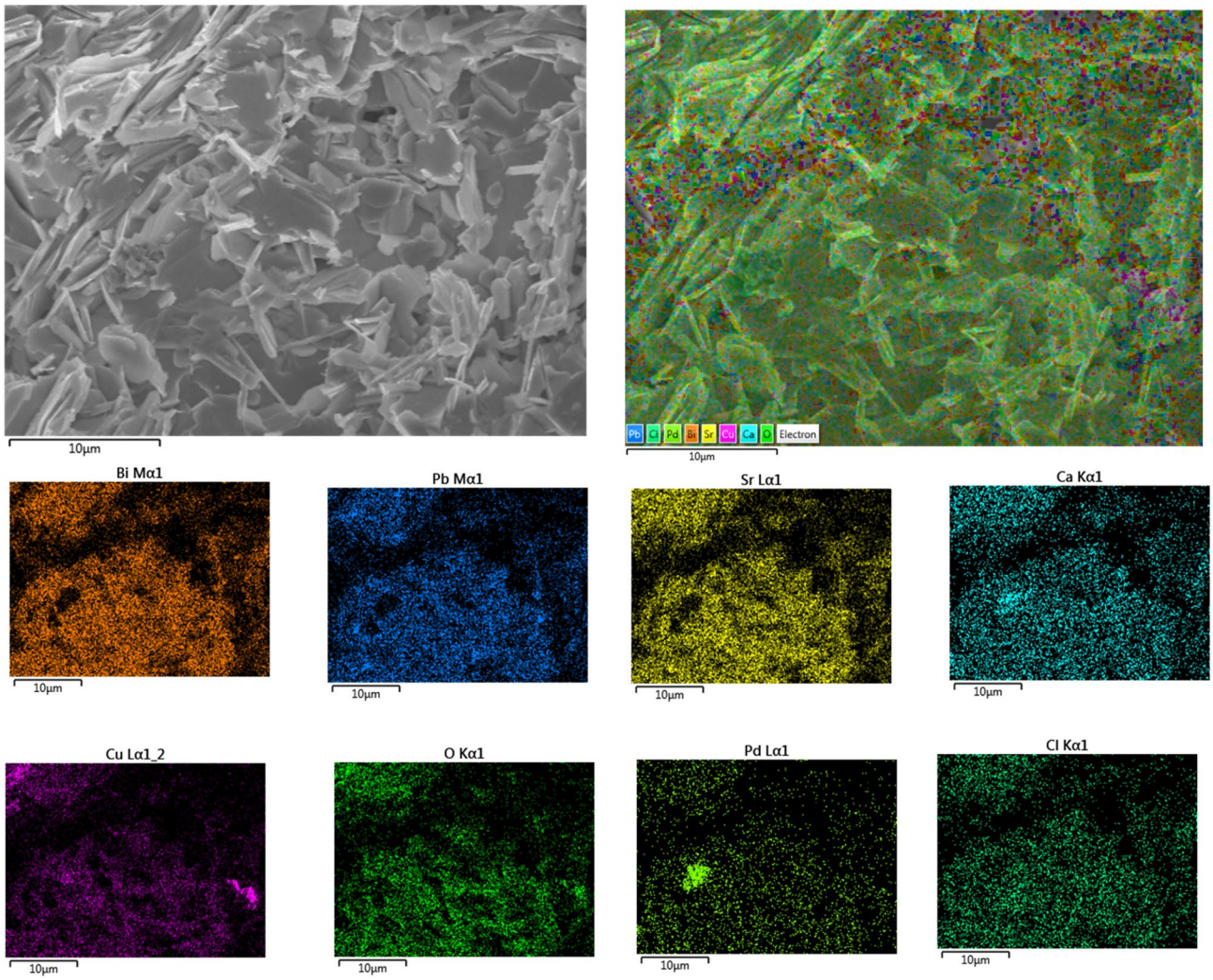

Fig. 5 Elemental distribution map of $Bi_{1.6}Pb_{0.4}Sr_2CaCu_2O_8$ added with 0.4 wt% $PdCl_2$

The undoped sample exhibited $T_{c\ onset}$ and zero transition temperature ($T_{c\ zero}$) values of 82 and 71 K, respectively. All $PdCl_2$-added samples showed higher $T_{c\ onset}$ values (ranging from 87 to 96 K) compared to undoped sample. Meanwhile, the $T_{c\ zero}$ initially decreased for the lower $PdCl_2$ additions ($x = 0.1$ and 0.2 wt%), then increased significantly for 0.4 wt% $PdCl_2$-added sample, before slightly decreased again with further addition. The highest $T_{c\ onset}$ of 96 K and $T_{c\ zero}$ of 77 K were obtained for 0.4 wt% $PdCl_2$-added sample. Table 2 shows the transition width (ΔT_c) of the undoped sample was 11 K and it broadened with increasing $PdCl_2$ addition. The broadening of ΔT_c indicates the inhomogeneities of T_c for the individual grains increased with $PdCl_2$ addition. This finding is consistent with the room-temperature resistivity (ρ_{300} K) results, where the addition of $PdCl_2$ increased the room-temperature resistivity of Bi-2212 (Table 2). The higher resistivity is attributed to the formation of secondary impurity phases, as confirmed by the XRD results (Fig. 1), and to weak coupling between superconducting grains.

Figure 7 shows the derivative (dR/dT) versus temperature curves for $Bi_{1.6}Pb_{0.4}Sr_2CaCu_2O_8$ samples with x wt% $PdCl_2$ additions (x = 0.0, 0.2 and 0.4 wt%). The first peak (T_c^{p1}) at higher temperature corresponds to the onset of superconductivity within the grains, while the grain boundaries remain in the normal state. The second peak (T_c^{p2}) at lower temperature corresponds to the temperature at which supercurrent flows between grains, indicating that the grain boundaries have also transitioned to the superconducting state.

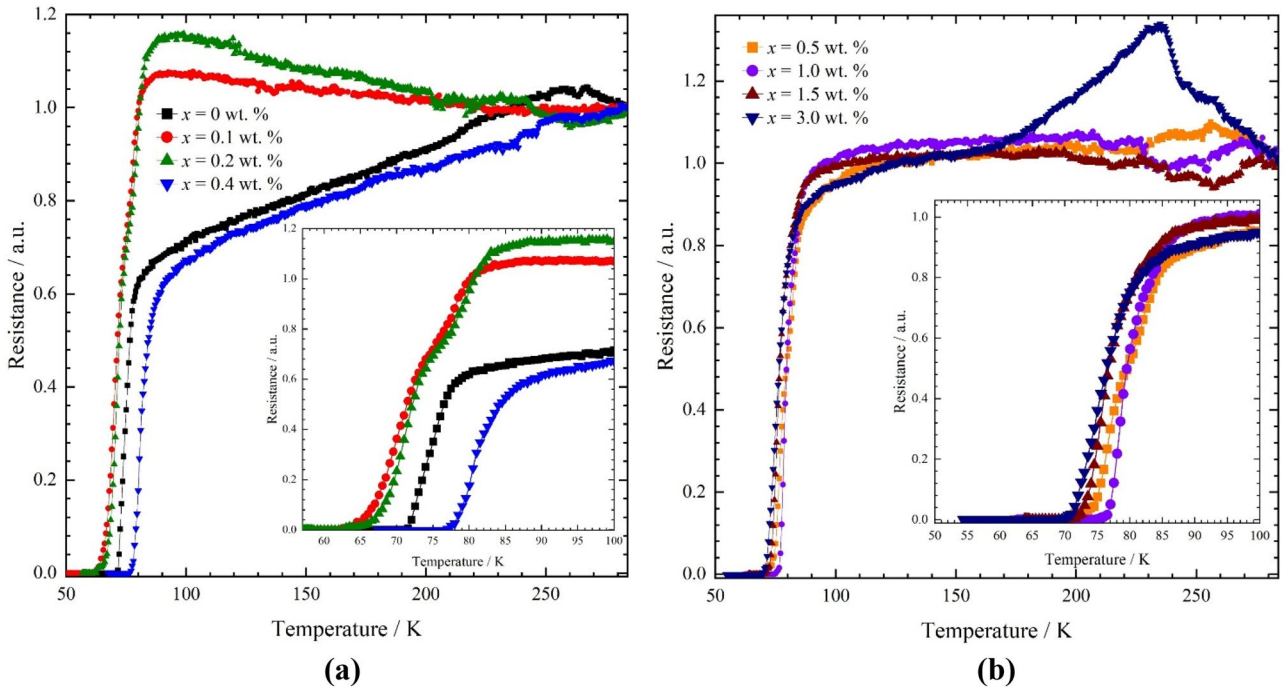

Fig. 6 Normalised resistance versus temperature of $Bi_{1.6}Pb_{0.4}Sr_2CaCu_2O_8$ with $PdCl_2$ additions of **a** $x = 0.0$, 0.1, 0.2, and 0.4 wt% **b** $x = 0.5$, 1.0, 1.5, and 3.0 wt%

Table 2 $T_{c\ onset}$, $T_{c\ zero}$, ΔT_c, T_c^{p1}, $T_{cp}{}^2$ and $\rho_{300\ K}$ of $Bi_{1.6}Pb_{0.4}Sr_2CaCu_2O_8$ samples with x wt% $PdCl_2$ additions

Sample/wt%	$T_{c\ onset}$/ K	$T_{c\ zero}$/ K	ΔT_c/ K	$T_c{}^{p1}$/ K	$T_c{}^{p2}$/ K	$\rho_{300\ K}$/ mΩ-cm
0	82	71	11	76	73	3.09
0.1	90	62	28	78	70	11.24
0.2	89	63	26	80	71	11.57
0.4	96	77	19	81	-	4.05
0.5	91	71	20	82	77	6.21
1.0	92	75	17	85	79	9.21
1.5	94	70	24	81	76	7.99
3.0	87	70	17	-	75	22.19

All samples exhibited two peaks, except for x = 0.4 and 3.0 wt% samples, which showed a single peak. This indicates that superconductivity occurs simultaneously within grains and across grain boundaries, likely due to the improved microstructure observed in the SEM image (Fig. 2). The plate-like grains with high aspect ratio in 0.4 wt% $PdCl_2$-added sample enhanced intergrain coupling by reducing grain boundary area and minimising weak-link effects leading to better current flow between the grains [31]. This behavior can be explained by the Brick Wall (BW) model [32, 33]. According to the BW model, when ab-plane conduction is hindered, the large surface area of basal-plane-faced grain boundaries generated by elongated, high aspect ratio grains allow for substantial c-axis supercurrent coupling. This model emphasises that optimised grain structure improves current transport pathways, resulting in an increase in the critical current density across the Bi-2212 samples.

The $T_c{}^{p1}$ and $T_c{}^{p2}$ for undoped sample were 76 and 73 K, respectively. All $PdCl_2$-added samples exhibited higher $T_c{}^{p1}$ values compared to undoped samples. The enhancement of $T_c{}^{p2}$ was more pronounced at higher $PdCl_2$ additions ($x = 0.5$–3.0 wt%.). However, the difference between $T_c{}^{p1}$ and $T_c{}^{p2}$ for all $PdCl_2$-added samples was generally larger compared to the undoped sample. This indicated that the weak-link behavior in Bi-2212 increased with $PdCl_2$ addition [34].

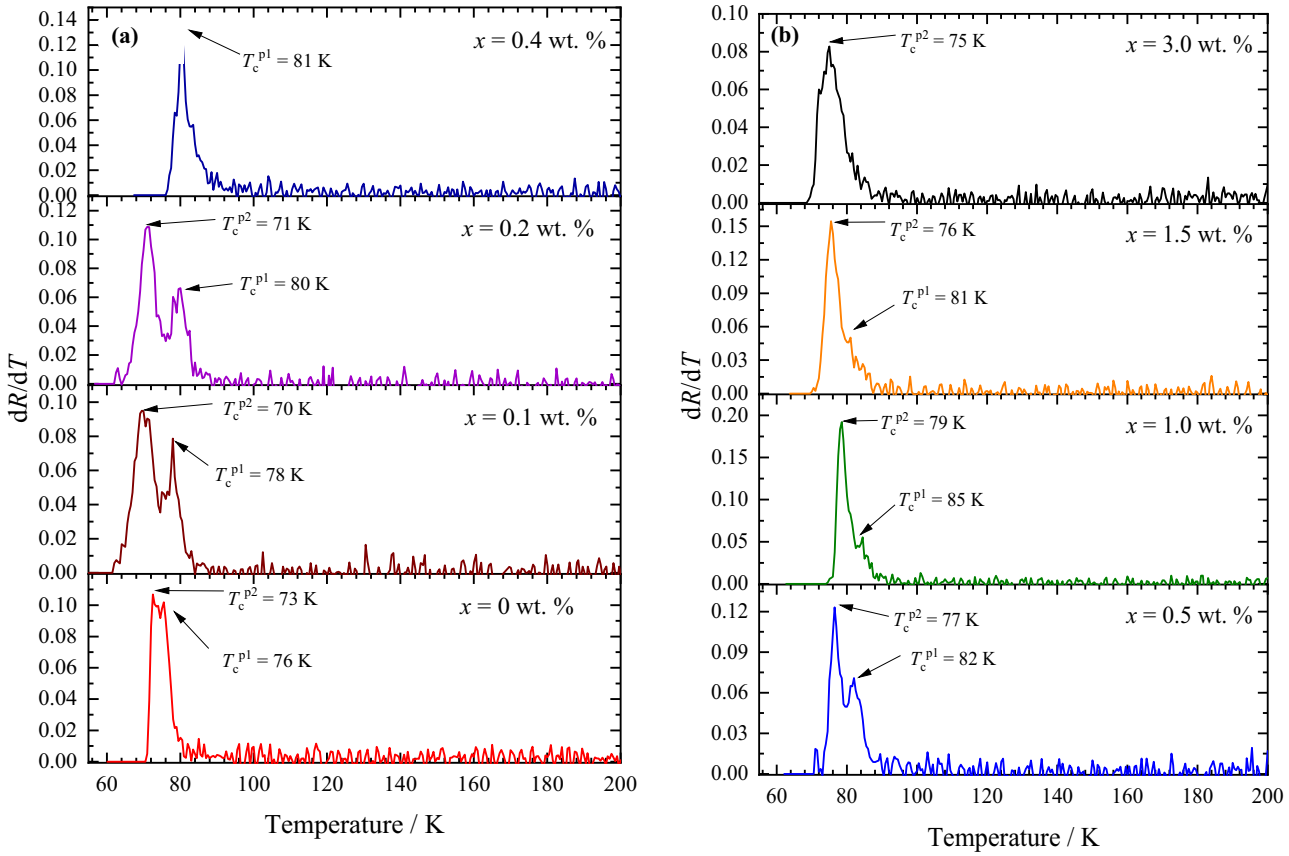

Fig. 7 **a** dR/dT versus temperature of $Bi_{1.6}Pb_{0.4}Sr_2CaCu_2O_8$ added with x wt% of $PdCl_2$ **b** dR/dT versus temperature of $Bi_{1.6}Pb_{0.4}Sr_2CaCu_2O_8$ added with x wt% of $PdCl_2$

3.4 AC susceptibility analysis

AC susceptibility curves for all samples are shown in Fig. 8. The real part of the susceptibility (χ') provides information about the paramagnetic-diamagnetic transition, also referred to as susceptibility transition temperatures ($T_{c\chi'}$), which is identified as the point where the straight line begins to deviate. The $T_{c\chi'}$ values for all samples ranged from 76 to 86 K. All $PdCl_2$-added samples exhibited higher $T_{c\chi'}$ values compared to the undoped sample, with the highest $T_{c\chi'}$ = 86 K observed for x = 1.0 and 1.5 wt% samples.

The imaginary part of the susceptibility (χ'') exhibited two peaks: the first peak at higher temperature corresponds to intragrain (intrinsic) losses, while the second peak at lower temperature is associated with intergrain losses. Intrinsic loss peaks were observed in x = 0.1 and 0.2 wt% samples (Fig. 8a), indicating flux penetration within the grains. The temperature for intrinsic losses peak (T_{p1}) for both samples was 79 K. No T_{p1} was observed in other samples.

Interestingly, all samples exhibited intergrain losses peak (T_{p2}) except for x = 0.1 and 0.2 wt% (Fig. 8). It is possible that the intergrain loss peaks for these samples occur below 20 K. The temperature of T_{p2} for undoped (0.0 wt%) and $x \geq 0.4$ wt% samples ranged between 45 and 69 K. The highest T_{p2} (69 K) obtained for x = 0.4 wt% sample. This finding aligns with the SEM microstructure analysis, which revealed larger grain size in the x = 0.4 wt% sample compared to undoped sample. This indicated that the intergrain coupling was significantly enhanced in the x = 0.4 wt% sample.

The critical current density (J_c) at the intergrain loss peak temperature (T_{p2}) of the imaginary component of the AC susceptibility was estimated using Bean's critical state model [35]:

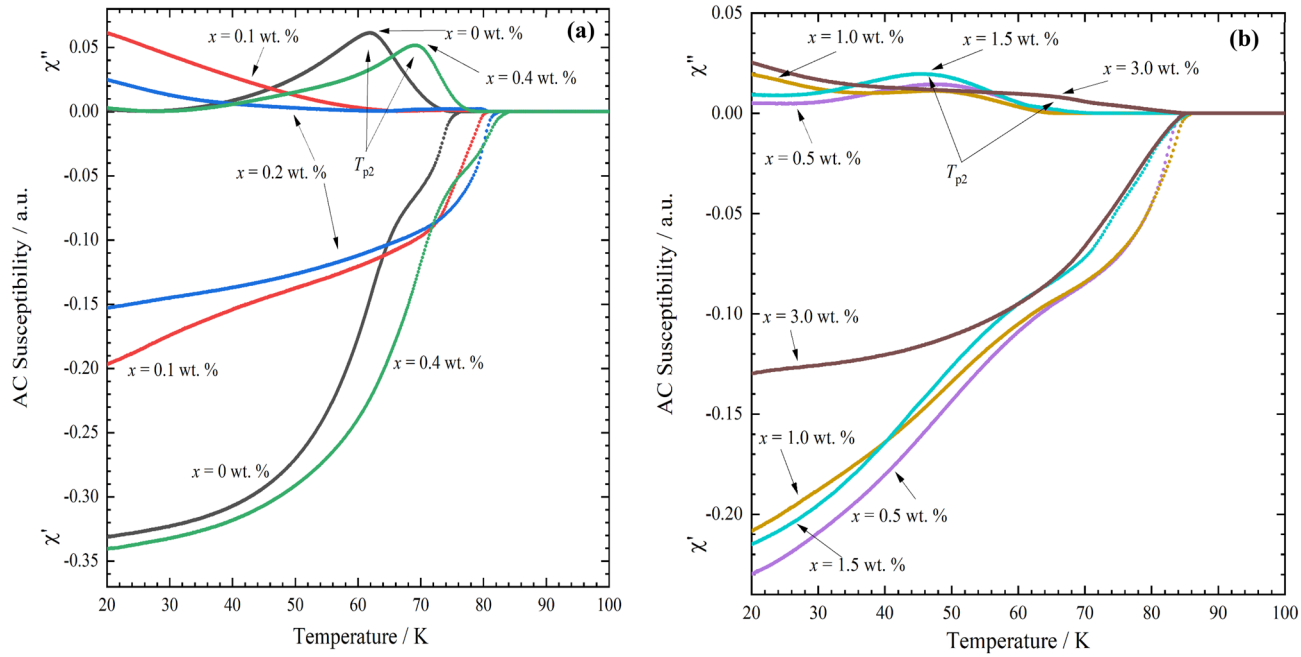

Fig. 8 **a** AC susceptibility of $Bi_{1.6}Pb_{0.4}Sr_2CaCu_2O_8$ added with x wt% of $PdCl_2$ (x=0.0, 0.1, 0.2, and 0.4 wt%). **b** AC susceptibility of $Bi_{1.6}Pb_{0.4}Sr_2CaCu_2O_8$ added with x wt% of $PdCl_2$ (x=0.5, 1.0, 1.5, and 3.0 wt%)

$$J_c(T_p) = \frac{H_{max}}{\sqrt{w}} \tag{4}$$

where H_{max} represents magnetic field corresponding to full magnetic flux penetration at T_{p2}, and w denotes the cross-sectional dimension of the bar-shaped samples. The calculated $J_c(T_p)$ values for all samples ranged from 14 to 17 A.cm^{-2}, as summarized in Table 3.

High-T_c superconductors are well known to consist of grains separated by weakly coupled boundary layers. The current crossing these boundaries (weak links) behaves as a Josephson current. The maximum Josephson current (I_0) across grain boundaries can be estimated from the phase-locking temperature (T_{cj}), which corresponds to the onset of grain decoupling and is associated with the lower transition temperature. It can be calculated using equation [36]:

$$I_0 = 1.57 \times 10^{-8} \times \left(\frac{T^2_{c\chi'}}{T_{c\chi'} - T_{cj}} \right) \tag{5}$$

The Josephson coupling energy (E_j) can be expressed by the following equation:

$$E_j = \left(\frac{h}{4\pi e} \right) I_0 \tag{6}$$

where h is Planck's constant and e is the elementary charge. The phase locking temperature, (T_{cj}),

Table 3 $T_{c\chi'}$, T_{p1}, T_{p2}, T_{cj}, I_0 and E_j of $Bi_{1.6}Pb_{0.4}Sr_2CaCu_2O_8$ samples with x wt% $PdCl_2$ additions

Sample/ wt.%	$T_{c\chi'}$/ K	T_{p1}/ K	T_{p2}/ K	T_{cj}/ K	I_o/ μA	E_j/ meV	$J_c(T_p)$/ A.cm^{-2}
0	76	-	62	62	6.48	13.31	17
0.1	81	79	<20	76	20.60	42.32	17
0.2	83	79	<20	80	36.05	74.06	17
0.4	84	-	69	70	7.91	16.26	14
0.5	85	-	47	47	2.99	6.13	16
1.0	86	-	48	52	3.42	7.02	16
1.5	86	-	45	44	2.76	5.68	16
3.0	85	-	64	77	14.18	29.13	14

indicating the beginning of grain decoupling, was determined from the peak position of the dχ'/dT curve (Fig. 8). The T_{cj} values for all samples ranged from 44 to 80 K, with the highest value of 80 K observed for 0.2 wt% $PdCl_2$-added sample. All key parameters obtained from χ' and χ'' curves including $T_{c\chi'}$, T_{p1}, T_{p2}, T_{cj}, I_0 and E_j are listed in Table 3. For the undoped samples, I_0 and E_j were 6.48 μA and 13.31 meV, respectively. Both parameters increased with $PdCl_2$ addition up to x = 0.2 wt%, followed by a gradual decrease up to x = 1.5 wt% and subsequent increase at x = 3.0 wt%. The highest I_0 and E_j values were obtained for 0.2 wt% $PdCl_2$-added sample, indicating enhanced grain connectivity. It is noteworthy that 3.0 wt% $PdCl_2$-added sample also exhibited higher I_0 and E_j than the undoped sample, suggesting that the higher $PdCl_2$ content can reinforce intergranular coupling of the sample.

4 Conclusions

In conclusion, the effect of palladium (II) chloride ($PdCl_2$) addition on the structural, microstructural, and superconducting properties of $Bi_{1.6}Pb_{0.4}Sr_2CaCu_2O_8$ were investigated. XRD results showed the Bi-2212 phase is dominant for all samples. The lattice parameters and unit cell volume decreased with $PdCl_2$ addition. SEM analysis revealed the plate-like grains in the added samples as compared to undoped one. The onset transition temperature ($T_{c\ onset}$) and susceptibility transition temperatures ($T_{c\chi'}$) for $PdCl_2$-added samples showed a higher value compared to undoped sample. The 0.4 wt% $PdCl_2$-added sample exhibited the highest $T_{c\ onset}$ of 96 K and zero-resistance transition temperature ($T_{c\ zero}$) of 77 K. In addition, this sample also showed the highest T_{p2} value, indicating enhanced flux pinning strength within the Bi-2212 phase. The samples with x = 1.0 and 1.5 wt% displayed the highest $T_{c\chi'}$ of 86 K. Future work could investigate the effects of other metal chloride additions and further optimize the synthesis parameters to improve the superconducting performance of Bi-2212.

Author contributions

Conceptualisation: M.A. Salma, S.K. Chen, and R. Abd-Shukor; Methodology: M.A. Salma, and A.B.P. Ilhamsyah; Formal analysis: M.A. Salma, and A.B.P. Ilhamsyah; Writing—original draft preparation: M.A. Salma, and A.B.P. Ilhamsyah; Writing—review and editing: R. Abd-Shukor, S.K. Chen, N.M. Hapipi, R. Che Hak, and H. Baqiah; Supervision: S.K. Chen, and R. Abd-Shukor; Funding acquisition: S.K. Chen, R. Abd-Shukor, M.M. Awang Kechik, and K.P. Lim.

Funding

Open access funding provided by The Ministry of Higher Education Malaysia and Universiti Putra Malaysia. Funding was provided by Ministry of Higher Education (MoHE) Malaysia through the Fundamental Research Grant Scheme, FRGS/1/2023/STG05/UPM/02/6

Data availability

Data will be made available on request.

Declarations

Conflict of interest The authors declare no competing interests.

References

1. M.A. Rahman, M.Z. Rahaman, M.N. Samsuddoha, Am. J. Phys. Appl. **3**, 39–56 (2015)
2. S.H. Mahdi, F.M. Salim, K.A. Jasim, M.A. Ali, S.A. Ahmed, N.Q. Fadhel, A.I.P. Conf, Proc. **1968**, 030043 (2018)
3. A. Jeremie, K. Alami-Yadri, J.C. Grivel, R. Flükiger, Supercond. Sci. Technol. **6**, 730 (1993)
4. W.M. Faisal, S.K.J. Al-Ani, Int. J. Phys. Sci. **7**, 171 (2012)
5. M. Yavuz, H. Maeda, L. Vance, H.K. Liu, S.X. Dou, J. Alloys Compd. **281**, 280–289 (1998)
6. A. Jeremie, J.C. Grivel, R. Flükiger, Physica C **235–240**, 943–944 (1994)
7. V.P.S. Awana, S.K. Agarwal, R. Ray, S. Gupta, A.V. Narlikar, Physica C **191**, 43–51 (1992)
8. M.C. Cheng, B.P. Yan, K.H. Lee, Q.Y. Ma, E.S. Yang, Supercond. Sci. Technol. **18**, 1100 (2005)
9. D.W. Ha, S.C. Kim, J.G. Oh, H.S. Ha, N.J. Lee, K.J. Song, T.H. Kim, R.K. Ko, H.S. Kim, S.K. Park, S.K. Lee, Y.M. Roh, S.S. Oh, IEEE Trans. Appl. Supercond. **17**, 3099–3102 (2007)
10. K. Habanjar, A. Younes, W. Labban, R. Awad, J. Mater. Sci. Mater. Electron. **34**, 2275 (2023)
11. T. Masuda, T. Kato, H. Yumura, M. Watanabe, Y. Ashibe, K. Ohkura, C. Suzawa, M. Hirose, S. Isojima, K. Matsuo, S. Honjo, T. Mimura, T. Kuramochi, Y. Takahashi, H. Suzuki, T. Okamoto, Physica C **378–381**, 1174–1180 (2002)
12. H. Miao, Y. Huang, S. Hong, J.A. Parrell, IEEE Trans. Appl. Supercond. **23**, 6400104 (2013)
13. G. Deutscher, In Highlights, in *Condensed Matter Physics and Future Prospects*. ed. by L. Esaki (Springer, Boston, 1991), pp.399–413
14. A. Sedky, Physica C **468**, 1041–1046 (2008)
15. K.M. Elsabawy, A.M. Fallatah, Z.O. Owidah, SN Appl. Sci. **3**, 408 (2021)
16. C. Shih-Yun, C. In-Gann, Supercond. Sci. Technol. **17**, 71 (2004)
17. D. Göhring, M. Vogt, W. Wischert, S. Kemmler-Sack, Mater. Sci. Eng. B Solid-State Mater. Adv. Technol. **48**, 244–253 (1997)
18. M. Yoshida, N. Ogawa, I. Hirabayashi, S. Tanaka, Physica C **185–189**, 2409–2410 (1991)
19. A. Veneva, I. Iordanov, L. Toshev, A. Stoyanova-Ivanova, D. Gogova, Physica C **308**, 175–184 (1998)
20. K.H. Yoon, S.S. Chang, J. Appl. Phys. **67**, 2516–2519 (1990)
21. M. Chen, Z. Liu, M. Li, Z. Yan, R. Huang, S. Qian, J. Chen, C. Cai, Crystals **12**, 925 (2022)
22. M. Noro, H. Andoh, H. Murotani, T. Sugiura, T. Tsukamoto, Phys. Procedia **27**, 148–151 (2012)
23. V. Mihalache, G. Aldica, P. Badica, Physica C **392–396**, 185–188 (2003)
24. R.T. Pardasani, P. Pardasani, in *Magnetic Properties of Paramagnetic Compounds*. ed. by A. Gupta (Springer-Verlag, Heidelberg, 2017), p.31D
25. K. Chawla, D. Kumar Yadav, A. Bajpai, S. Kumar, I.P. Jain, C. Lal, Sustain. Energy Technol. Assess. **51**, 101981 (2022)
26. J. O'Neil, P.E. Heckelman, C.B. Koch, K.J. Roman, *The merck index: An encyclopedia of chemicals, drugs, and biologicals* (Merck & Co., Whitehouse Station, NJ, 2001)
27. L. Shlyk, G. Krabbes, G. Fuchs, G. Stöver, S. Gruss, K. Nenkov, Physica C **377**, 437–444 (2002)
28. G. Ferey, A. Le Bail, Y. Laligant, M. Hervieu, B. Raveau, A. Sulpice, R. Tournier, J. Solid State Chem. **73**, 610–614 (1988)
29. R.D. Shannon, Acta Crystallogr. Sect. A **32**, 751–767 (1976)
30. J.I. Langford, A.J.C. Wilson, J. Appl. Crystallogr. **11**, 102–113 (1978)
31. S.N. Abdullah, M.M. Kechik, A.N. Kamarudin, Z.A. Talib, H. Baqiah, C.S. Kien, L.K. Pah, M.K. Abdul Karim, M.K. Shabdin, A.H. Shaari, A. Hashim, N.E. Suhaimi, M. Miryala, Nanomaterials **13**, 2197 (2023)
32. L.N. Bulaevskii, L.L. Daemen, M.P. Maley, J.Y. Coulter, Phys. Rev. B **48**, 13798–13816 (1993)
33. L.N. Bulaevskii, J.R. Clem, L.I. Glazman, A.P. Malozemoff, Phys. Rev. B **45**, 2545–2548 (1992)
34. A.B.P. Ilhamsyah, N.A.M. Zabidi, M.A.H. Hashidi, N.R.M. Suib, A.M. Mahat, R. Abd-Shukor, M.J. Masnita, Appl. Phys. A **130**, 590 (2024)
35. C.P. Bean, Rev. Mod. Phys. **36**, 31–39 (1964)
36. J.R. Clem, Physica C **153–155**, 50–55 (1988)